tektonika

Supporting Information

For

Impact of material strength on releasing bend evolution

Alana M. Gabriel[1], Hanna M. Elston[1], Michele L. Cooke[1] and Christ F. Ramos Sánchez[1]*

[1] Earth, Geographic and Climate Sciences, University of Massachusetts Amherst, USA
**corresponding author (email: alana.gabriel16@gmail.com)*

Contents

Gabriel et al (2025) - https://doi.org/10.55575/tektonika2025.3.1.81

1. Structure from Motion measures topography

We employed Structure from Motion to capture the topography of the clay surface at regular intervals throughout the experiments of this study. Because the subsidence and uplift caused by dip slip along faults and off-fault deformation is on the order of a few millimeters, we require fine vertical resolution of elevation. In this study, we used Structure from Motion from Agisoft Metashape Professional Edition, which uses images from several cameras and ground control points to reliably capture fine changes in topography of laboratory experiments (e.g., Bonali et al., 2019; Cawood and Wyrick, in review; Galland et al., 2016; Von Hagke et al., 2019). Other approaches that use images from two cameras, such as Stereovision, can be challenging to calibrate (e.g., Toeneboehn et al., 2018). Metashape™ allows users to efficiently calibrate all cameras and process digital images to generate three-dimensional spatial data in the form of dense point clouds based on depth maps calculated using dense stereo matching.

For each basal plate displacement of interest in the experiments, the Metashape™ processing evaluates photos from all five camera locations and the known x, y and z coordinates of each control point (Figure S1). The Structure from Motion algorithm uses overlapping images and coordinate system provided by the control points to calculate multiple pairwise depth maps through dense stereo matching (e.g., Bemis et al., 2014). Noise reduction in the image overlap region yields a single depth map for each camera. Lastly, Metashape™ merges all depth maps from each camera to generate the final dense point cloud with over several million data points for the experimental surface.

Using Matlab™, we cropped, interpolated and smoothed the dense point cloud to the region of interest to produce a high-resolution surface map that allowed for the analysis of the subsidence/uplift during the experiments. Cropping the dense point cloud to the releasing bend area reduced the number of points to ~1.2 million. The interpolation of the scattered points into a regular grid with 0.2 mm spacing produces a comparable number of gridded data points at the scattered point cloud. We assessed error from the observed variation in detected elevation of the clay surface along transects far from the releasing bend basin that do not have fault related elevation changes. We removed any overall subtle slopes by detrending the elevation data. Prior to smoothing, the surface elevation at points far from the basin in the stronger clay experiment had sharp spikes that deviated up to 1mm from the overall surface elevation (Figure S1 b & c). The 3-point median filter

Gabriel et al (2025) - https://doi.org/10.55575/tektonika2025.3.1.81

removes the spikes and produced a surface with <0.5 mm variation in elevation (Figure S1 e &f). The weaker experiment also showed local variations less than <0.5 mm (Figure S1). The east-west transects of the weaker clay experiment also showed great subsidence in the center of the claybox than the same transects in the stronger clay experiment. We used the elevation information to investigate the shape of the clay surface at the end of the experiment.

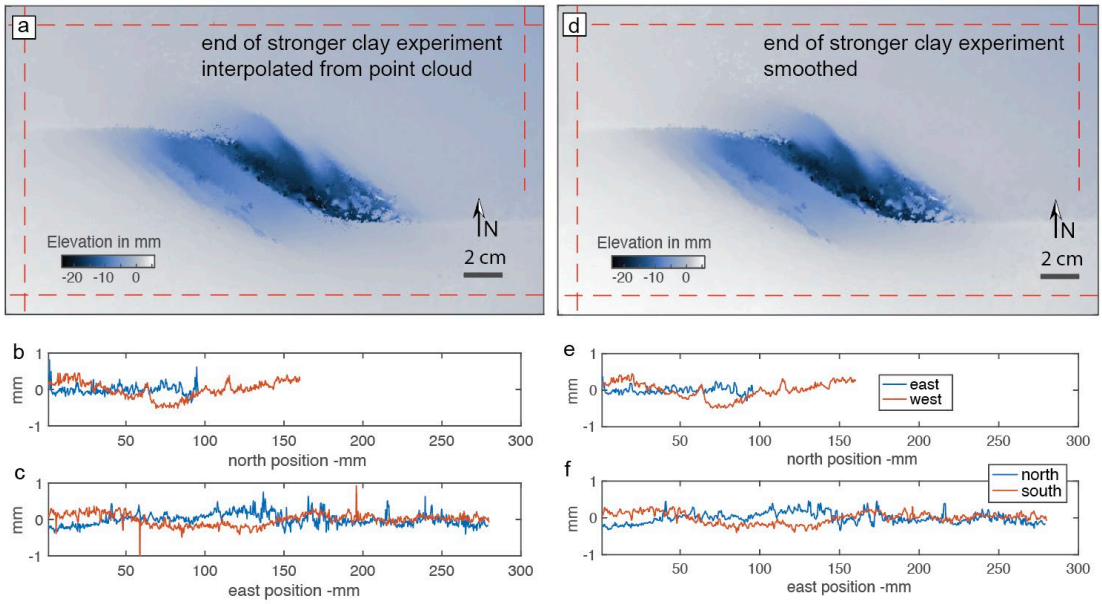

Figure S1. *Transects across the elevation map far from the releasing bend at the end of the stronger experiment reveal the elevation errors from Structure from Motion point cloud (a,b &c) and after smoothing (d,e&f). a&d) elevation maps show transect locations in red dashed lines. The eastern transect was abbreviated to avoid elevation changes associated with the fault. b,c, e &f) Elevation transects were linearly-detrended to remove subtle slope of the clay surface. The detected surface elevation variations along transects far from the basin reflect the errors of the elevation estimates.*

Gabriel et al (2025) - https://doi.org/10.55575/tektonika2025.3.1.81

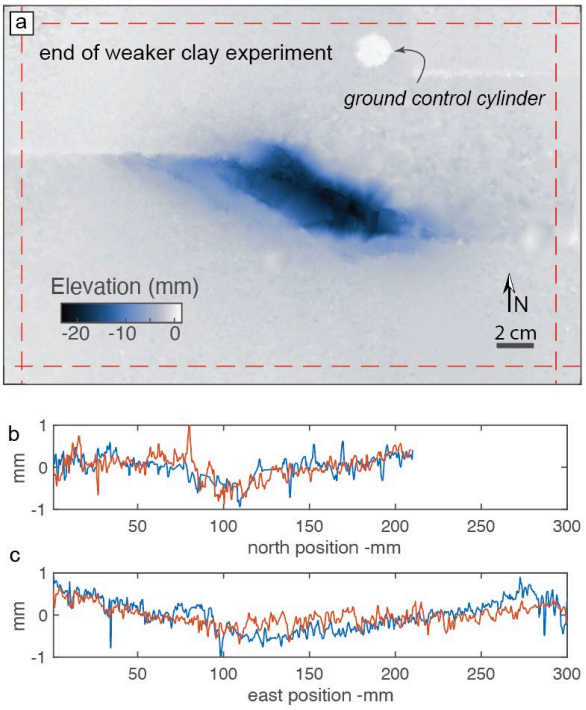

Figure S2. *Transects across the elevation map far from the releasing bend at the end of the weaker experiment reveal the elevation errors from Structure from Motion point cloud after smoothing. a) elevation maps show transect locations in red dashed lines. b &d) Elevation transects were linearly-detrended to remove subtle slope of the clay surface. The detected surface elevation variations along the transects that are far from the basin reflect the errors of the elevation estimates.*

2. Repeated experiments

We conduct a second set of experiments with identical conditions as the first set to assess the repeatability of the releasing bend fault evolution. The wet kaolin of the stronger experiment had undrained shear strength of 109.6± 2.0 Pa and the weaker experiment had strength of 81.2 ±1.0 Pa. The data repository hosts strain animations of all experiments include the repeated experiments described here (Gabriel et al., 2024).

Gabriel et al (2025) - https://doi.org/10.55575/tektonika2025.3.1.81

2.1 Stronger Clay Experiment Fault Evolution

The repeated stronger clay experiment showed similar fault evolution to the original stronger clay experiment, except for early irregularity along the releasing bend segment and the additional development of short-lived cross faults.

2.1.1 Spin up period

Starting at 6 mm of plate displacement, the right-lateral slip along the precut releasing bend is distributed along two parallel surfaces. When we cut the vertical fault, we move the probe along the surface in one direction and then travel back along the same path using a template to guide the probe. The emergence of two early precut faults reflects that the probe did not return along exactly the same path the second time. By 15 mm of plate displacement, slip along precut surfaces had merged along a single fault at the top of the claypack.

2.1.2 Early Stage 1 (12-16mm plate displacement)

Similar to the original stronger clay experiment, secondary normal faults that trend subparallel to the releasing segment develop above the moving and stationary plates. Some of the new faults connected directly to the precut and some did not. Where the secondary faults connect to the precut, the faults accommodated primarily right-lateral rather than normal slip.

2.1.3 Late Stage 1 (16-35mm plate displacement)

Throughout stage 1, activity on normal faults above the stationary plate migrated basinward; older faults ceased slipping when new faults developed. Different from the original stronger clay experiment, a short-lived cross fault developed from 16-18mm displacement connecting the secondary fault above the moving plate to the eastern kink of precut. Throughout the later part of stage 1, the secondary faults above the moving fault accommodated increasing component of right-lateral slip. By the end of stage 1 only one primarily right-lateral secondary fault was active above the moving plate.

2.1.4 Stage 2 (35-60 plate displacement)

Reorganization of the primary slip pathway started with the growth of new right-lateral faults that connected the tip of the secondary fault above the moving plate to the western kink of the precut to form a second throughgoing pathway. From 44-56 mm plate displacement, two short-lived cross faults developed to connect the precut releasing

Gabriel et al (2025) - https://doi.org/10.55575/tektonika2025.3.1.81

segment and the secondary fault near the western kink. Starting at 44 mm displacement, regions of the precut releasing segment ceased slipping. With the cessation of slip along the precut fault surface, the secondary fault above the moving plate became the primary slip pathway. The precut releasing segment ceased slipping entirely by 60 mm displacement at which point, the secondary fault was the only throughgoing pathway.

The photographs at the end of the experiment revealed the sand-free fault scarp of the originally vertical precut releasing bend segment. The exposure of the fault surface to overhead camera shows that the dip of the precut fault surface had shallowed by the end of the experiment and was no longer vertical.

2.2 Weaker clay experiment Fault Evolution:

The repeated weaker experiment had similar fault evolution as the original experiment described in the main text of the paper.

2.2.1 Stage 1 (8-21mm plate displacement)

During stage 1, right lateral secondary faults developed above both the stationary and moving plates but the fault above the stationary fault was much shorter lived and shorter in length. At about 10 mm of plate displacement, several small right-lateral faults initiated along the precut above the stationary fault and by 15 mm of plate displacement had strain had localized onto a single secondary fault. This fault ceased slipping by 20mm plate displacement. One right-lateral secondary fault developed above the moving plate and propagated northwest throughout stage 1. As the fault lengthened, the northwest portion of this fault, which had more northerly trend than the rest of the secondary fault, showed left-lateral slip by 15mm displacement. At the end of stage one, the precut releasing bend was the only throughgoing slip pathway.

2.2.2 Stage 2 (22-60mm plate displacement)

Left-lateral cross faults developed above the moving plate at 22 mm plate displacement. One cross fault connected the tip of the secondary fault and the precut releasing segment. During stage 2, the secondary fault continued to propagate northwestward and the end of the fault farthest from the precut accommodated primarily left-lateral slip. At 32 mm plate displacement new left-lateral faults with more westerly trend than the cross faults developed above the western kink. Cross faults continued to form that connected subparallel secondary faults and the releasing segment. A complex zone of faulting

developed for the remainder of the experiment as the cross faults and other secondary faults connected the secondary fault and portions of the precut fault. At 26 mm plate displacement, a series of 1-2 cm long subparallel normal faults developed above the stationary plate. Beginning at 35 mm basal plate displacement, sections of the precut releasing segment ceased slipping followed by the development of new right-lateral faults at the western kink that connected the precut strike-slip fault with the secondary faults. Continuing until 56 mm plate displacement, slip ceased on the releasing segment in different regions and the secondary fault formed a new throughgoing slip pathway through the releasing bend.

The photographs at the end of the experiment revealed the sand-free fault scarp of the originally vertical precut releasing bend segment. The exposure of the fault surface to overhead camera shows that the dip of the precut fault surface had shallowed by the end of the experiment and was no longer vertical. The repeated weaker clay experiment reveals greater fault scarp than the repeated stronger clay experiment, suggesting that the fault had greater change in dip within the weaker experiment.

2.3 Assessed Variation and Repeatability Implications:

The evolution of releasing bend faults is similar in the repeated experiments to the experiments presented in the primary text. First, the weaker clay experiments are similar and therefore repeatable in the degree of fault complexity including geometry and fault orientations. Major reorganizations occur in both experiments. The stronger clay experiments retain similarities when compared with the weaker clay experiments. The repeated experiment developed four short-lived cross faults near the kink, undergoes reorganization of the releasing segment and has a generally more complex geometry than the original experiment. The greater complexity of the repeated stronger clay experiment may owe to heterogeneities introduced in the cutting of the initial releasing bend fault surface. However, the repeated stronger clay experiment has more localized faulting along fewer fault segments than either of the weaker clay experiment. While short-lived cross faults can develop in stronger clay, they are limited to regions with closely-spaced right-lateral faults and play a lesser role in the fault evolution than longer-lived cross-faults in the weaker experiments, which are active for 20-25 mm of plate displacement and have direct impact reorganization of the primary slip surface. Off-fault deformation between the kinks

and secondary faults may be higher allowing the development of the otherwise non-optimally orientated cross faults.

References

Bemis, S.P., Micklethwaite, S., Turner, D., James, M.R., Akciz, S., Thiele, S.T., Bangash, H.A., 2014. Ground-based and UAV-Based photogrammetry: A multi-scale, high-resolution mapping tool for structural geology and paleoseismology. J. Struct. Geol. 69, 163–178. https://doi.org/10.1016/j.jsg.2014.10.007

Bonali, F.L., Tibaldi, A., Marchese, F., Fallati, L., Russo, E., Corselli, C., Savini, A., 2019. UAV-based surveying in volcano-tectonics: An example from the Iceland rift. J. Struct. Geol. 121, 46–64. https://doi.org/10.1016/j.jsg.2019.02.004

Cawood, A., Wyrick, D., in review. Enhancing Photogrammetric Reconstruction of Geologic Analog Models. AGU Earth Space Sci.

Galland, O., Bertelsen, H.S., Guldstrand, F., Girod, L., Johannessen, R.F., Bjugger, F., Burchardt, S., Mair, K., 2016. Application of open-source photogrammetric software MicMac for monitoring surface deformation in laboratory models. J. Geophys. Res. Solid Earth 121, 2852–2872. https://doi.org/10.1002/2015JB012564

Toeneboehn, K., Cooke, M.L., Bemis, S.P., Fendick, A.M., Benowitz, J., 2018. Stereovision Combined With Particle Tracking Velocimetry Reveals Advection and Uplift Within a Restraining Bend Simulating the Denali Fault. Front. Earth Sci. 6, 152. https://doi.org/10.3389/feart.2018.00152

Von Hagke, C., Kettermann, M., Bitsch, N., Bücken, D., Weismüller, C., Urai, J.L., 2019. The Effect of Obliquity of Slip in Normal Faults on Distribution of Open Fractures. Front. Earth Sci. 7, 18. https://doi.org/10.3389/feart.2019.00018